AFRL-RQ-WP-TP-2014-0130

STUDY OF A MULTI-PHASE HYBRID HEAT EXCHANGER-REACTOR (HEX REACTOR): PART I – EXPERIMENTAL CHARACTERIZATION (POSTPRINT)

Nicholas Niedbalski and Debjyoti Banerjee

Texas A&M University

Douglas Johnson

University of Dayton Research Institute

Soumya S. Patnaik

Mechanical and Thermal Systems Branch
Power and Control Division

NOVEMBER 2013

AIR FORCE RESEARCH LABORATORY
AEROSPACE SYSTEMS DIRECTORATE
WRIGHT-PATTERSON AIR FORCE BASE, OH 45433-7542
AIR FORCE MATERIEL COMMAND
UNITED STATES AIR FORCE

NOTICE AND SIGNATURE PAGE

Using Government drawings, specifications, or other data included in this document for any purpose other than Government procurement does not in any way obligate the U.S. Government. The fact that the Government formulated or supplied the drawings, specifications, or other data does not license the holder or any other person or corporation; or convey any rights or permission to manufacture, use, or sell any patented invention that may relate to them.

This report was cleared for public release by the USAF 88th Air Base Wing (88 ABW) Public Affairs Office (PAO) and is available to the general public, including foreign nationals.

Copies may be obtained from the Defense Technical Information Center (DTIC) (http://www.dtic.mil).

AFRL-RQ-WP-TP-2014-0130 HAS BEEN REVIEWED AND IS APPROVED FOR PUBLICATION IN ACCORDANCE WITH ASSIGNED DISTRIBUTION STATEMENT.

*//Signature//

TRAVIS E MICHALAK
Program Manager
Mechanical and Thermal Systems Branch
Power and Control Division

//Signature//

THOMAS L. REITZ, Technical Advisor
Mechanical and Thermal Systems Branch
Power and Control Division
Aerospace Systems Directorate

//Signature//

JOHN G. NAIRUS, Chief Engineer
Power and Control Division
Aerospace Systems Directorate

This report is published in the interest of scientific and technical information exchange, and its publication does not constitute the Government's approval or disapproval of its ideas or findings.

*Disseminated copies will show "//Signature//" stamped or typed above the signature blocks.

REPORT DOCUMENTATION PAGE

Form Approved
OMB No. 0704-0188

1. REPORT DATE *(DD-MM-YY)*	2. REPORT TYPE	3. DATES COVERED *(From - To)*
November 2013	Journal Article Postprint	01 October 2011 – 28 May 2013

4. TITLE AND SUBTITLE
STUDY OF A MULTI-PHASE HYBRID HEAT EXCHANGER-REACTOR (HEX REACTOR): PART I – EXPERIMENTAL CHARACTERIZATION (POSTPRINT)

5a. CONTRACT NUMBER
In-house

5b. GRANT NUMBER

5c. PROGRAM ELEMENT NUMBER
62203F

6. AUTHOR(S)
Nicholas Niedbalski and Debjyoti Banerjee (Texas A&M University)
Douglas Johnson (University of Dayton Research Institute)
Soumya S. Patnaik (AFRL/RQQM)

5d. PROJECT NUMBER
3145

5e. TASK NUMBER
N/A

5f. WORK UNIT NUMBER
Q0LA

7. PERFORMING ORGANIZATION NAME(S) AND ADDRESS(ES)
Texas A&M University
Department of Mechanical Engineering
3123 TAMU
College Station, TX 77843

University of Dayton Research Institute
300 College Park
Dayton, OH 45469

Mechanical and Thermal Systems Branch (AFRL/RQQM)
Power and Control Division
Air Force Research Laboratory
Aerospace Systems Directorate
Wright-Patterson Air Force Base, OH 45433-7542
Air Force Materiel Command, United States Air Force

8. PERFORMING ORGANIZATION REPORT NUMBER
AFRL-RQ-WP-TP-2014-0130

9. SPONSORING/MONITORING AGENCY NAME(S) AND ADDRESS(ES)
Air Force Research Laboratory
Aerospace Systems Directorate
Wright-Patterson Air Force Base, OH 45433-7542
Air Force Materiel Command
United States Air Force

10. SPONSORING/MONITORING AGENCY ACRONYM(S)
AFRL/RQQM

11. SPONSORING/MONITORING AGENCY REPORT NUMBER(S)
AFRL-RQ-WP-TP-2014-0130

12. DISTRIBUTION/AVAILABILITY STATEMENT
Approved for public release; distribution unlimited.

13. SUPPLEMENTARY NOTES
PA Case Number: 88ABW-2013-2497; Clearance Date: 28 May 2013.

Report published in *International Journal of Heat and Mass Transfer* 70 (2014).

14. ABSTRACT
This study focuses on gaining fundamental insights into the sparsely explored area of reacting multiphase flows in a compact heat exchanger. Chevron plate heat exchangers have been demonstrated to possess superior thermal performance, scalability, and mixing capability compared to more traditional shell-in-tube heat exchangers or stirred tank batch reactors. This study explores the hydrodynamic behavior of gas-evolving reacting flows in chevron plate heat exchangers. Experimental characterization of a plate heat exchanger/chemical reactor (in multi-phase flow configuration) utilizing high-speed video and axial pressure measurements was conducted. Existing correlations that were developed using air–water flow in PHEs predicted with acceptable accuracy the total pressure drop in the HEX reactor.

15. SUBJECT TERMS
multi-phase flow, HEX Reactor, reacting flow, flow visualization, plate heat exchanger

16. SECURITY CLASSIFICATION OF:			17. LIMITATION OF ABSTRACT:	18. NUMBER OF PAGES	19a. NAME OF RESPONSIBLE PERSON (Monitor)
a. REPORT	b. ABSTRACT	c. THIS PAGE			Travis E. Michalak
Unclassified	Unclassified	Unclassified	SAR	14	19b. TELEPHONE NUMBER *(Include Area Code)* N/A

International Journal of Heat and Mass Transfer 70 (2014) 1078–1085

Contents lists available at ScienceDirect

International Journal of Heat and Mass Transfer

journal homepage: www.elsevier.com/locate/ijhmt

Study of a multi-phase hybrid heat exchanger-reactor (HEX reactor): Part I – Experimental characterization

Nicholas Niedbalski [a,b,*], Douglas Johnson [c], Soumya S. Patnaik [a], Debjyoti Banerjee [b]

[a] Air Force Research Laboratory, Aerospace Systems Directorate, Power and Controls Division, Mechanical and Thermal Systems Branch, 1950 5th St., WPAFB, OH 45433, United States
[b] Texas A&M University, Department of Mechanical Engineering, 3123 TAMU, College Station, TX 77843, United States
[c] University of Dayton Research Institute, 300 College Park, Dayton, OH 45469, United States

ARTICLE INFO

Article history:
Available online 16 November 2013

Keywords:
Multi-phase flow
HEX reactor
Reacting flow
Flow visualization
Plate heat exchanger

ABSTRACT

This study focuses on gaining fundamental insights into the sparsely explored area of reacting multiphase flows in a compact heat exchanger. Chevron plate heat exchangers have been demonstrated to possess superior thermal performance, scalability, and mixing capability compared to more traditional shell-in-tube heat exchangers or stirred tank batch reactors. This study explores the hydrodynamic behavior of gas-evolving reacting flows in chevron plate heat exchangers. Experimental characterization of a plate heat exchanger/chemical reactor (in multi-phase flow configuration) utilizing high-speed video and axial pressure measurements was conducted. Existing correlations that were developed using air–water flow in PHEs predicted with acceptable accuracy the total pressure drop in the HEX reactor.

1. Introduction

The concept of using a compact heat exchanger as a continuous flow chemical reactor, termed as heat exchanger (HEX) reactors, is well documented in the chemical engineering literature as discussed by Anxionnaz et al. [1]. The authors cite high volumetric heat transfer capacities ranging from 1400 to 4000 kW/m^3. This represents 2–3 orders-of-magnitude gain in the value of surface-area-to-volume-ratio when compared to that of batch reactors. Among the many classes of compact heat exchangers examined by these authors, the gasketed plate heat exchangers (PHEs) offer both high thermal performance and ease of maintenance. PHEs can be easily disassembled for inspection and maintenance (in contrast, shell-and-tube heat exchangers require very elaborate maintenance procedures due to the complexity of assembly/disassembly [1]). Also, the performance rating of a gasketed PHE can be scaled-up simply by assembling additional plates. The advantages of vigorous mixing, high surface area and low volume make the PHE-based HEX reactor an ideal platform for continuous delivery/removal of heat into/from a reacting multi-phase flow [2].

Although the continuous flow HEX reactor represents a promising approach to enhancing heat transfer in applications involving high energy density gas-evolving reactions, the hydrodynamics of combined multiphase flow and chemical reaction within a PHE are not well understood. Therefore, the motivation of this study is to gain insights into the nature of reacting multi-phase flows in a PHE serving as a HEX reactor. The objective of this paper is to establish an experimental basis for the hydrodynamics of gas-evolving reacting flows using a model chemical reaction, and to assess the accuracy and suitability of existing correlations for void fraction and pressure drop calculations in a chevron plate heat exchanger. The hydrodynamic correlations evaluated in this paper are used in Part II, which focuses on developing numerical models.

2. Experimental methods and materials

2.1. Chevron plate heat exchangers

Chevron PHEs consist of a stack of thin heat transfer plates with corrugated surfaces in the shape of a chevron (Fig. 1). These plates are separated by compliant gaskets, which, when the entire stack is mechanically compressed, seal the space in between a pair of mating plates to form channels. The gasket also serves to direct the cold/hot streams to their respective ports, as can be seen in Fig. 1. The chevron patterns of the upper and lower plates that form an individual channel face opposite directions to form a tortuous network of crisscrossing passageways. Fluid streams directed along the upper and lower corrugations interact to produce unique secondary flow patterns that give rise to enhanced convective heat transfer [3-5]. Additional details of the experimental set up and measurements are provided in an earlier study [2].

* Corresponding author at: A236, Building 18, 1950 5th St., Wright-Patterson AFB, OH 45433, United States. Tel.: +1 (425) 358 1295.
E-mail address: nickgonzaga@me.com (N. Niedbalski).

0017-9310/$ - see front matter © 2013 Elsevier Ltd. All rights reserved.
http://dx.doi.org/10.1016/j.ijheatmasstransfer.2013.10.066

Nomenclature

A	surface area
C	molar concentration
D	diameter
L	length
M	molecular weight
P	pressure
P_p	partial pressure
R_e	Reynolds number
T	temperature
U	superficial velocity
$\dot{V}$	volume flow rate
W	plate width (between gasket)
X	Lockhart–Martinelli parameter

Lowercases

d	½ Corrugation depth
f	Darcy friction factor
g	gravitational acceleration constant
k	rate constant
k^*	dimensionless rate constant
m''	gas-phase mass flux
$\dot{m}''_{total}$	total mass flux
t	time
u	velocity
x	mass quality
z	axial coordinate

Greek

Λ	corrugation pitch
Φ^2_{TP}	two-phase multiplier
α	void fraction
β	chevron angle
η	dimensionless concentration
ρ	density

Subscripts

A	acceleration
F	friction
G	gravity
SP	single-phase
TP	two-phase
c	corrugated section
e	equivalent
g	gas phase
h	hydraulic
l	liquid phase
pp	port-to-port

2.2. Experimental setup

The hydrodynamic effects of a solid–gas reacting flow was characterized using the well-known acid/base neutralization reaction between acetic acid and sodium bicarbonate:

$$NaHCO_3 + CH_3COOH \rightarrow CH_3COONa + H_2O + CO_2 \quad (1)$$

The reaction in Eq. (1) is non-toxic, and occurs at room temperature and atmospheric pressure; these attributes make acetic acid and sodium bicarbonate an ideal model reaction to study the hydrodynamics of gas-evolving multi-phase reacting flows.

The rate of reaction (and gas evolution) was controlled by varying the concentrations of the reactant species being fed through the reactor, and the reactor was run under adiabatic conditions. The overall reaction in Eq. (1) is first-order with respect to acetic acid [6] and is diffusion limited in aqueous solution [7]. Because of the high degree of mixing that occurs in PHEs, the concentration of the reactants is controlled so that the majority of the reaction is completed inside the channel, and the volume of gas produced can be determined directly from the molar concentrations of acetic acid and sodium bicarbonate introduced into the reactor.

The HEX reactor is an Alfa Laval MF3 gasketed chevron plate heat exchanger having the following dimensions, as detailed in Table 1.

To aid in flow visualization, the top plate of the channel was replaced with a transparent window fabricated from an acrylic casting resin (Electron Microscopy Sciences, Hatfield, PA). The resin was molded over one of the PHE heat transfer plates to form the chevron pattern, so as to preserve the channel geometry while

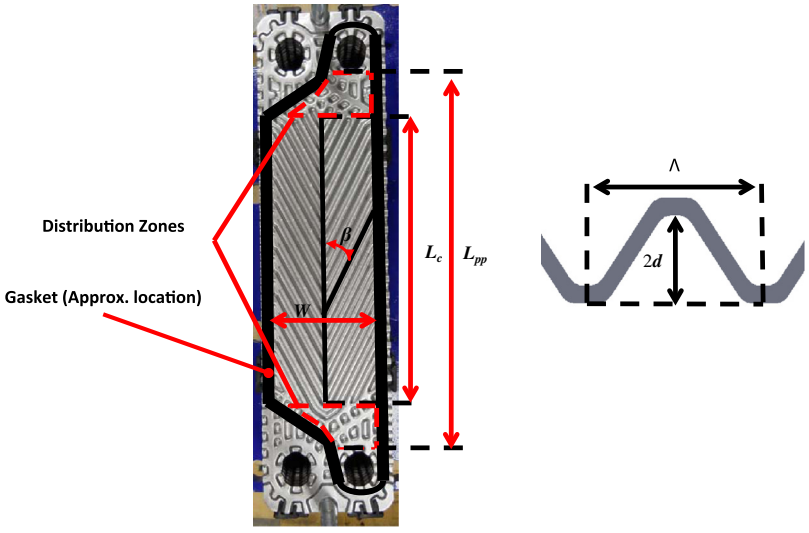

Fig. 1. Alpha Laval MF3 heat transfer plate used in this study (left) and profile of corrugation (right).

Table 1
Geometric data of Alfa Laval MF3 PHE.

Λ (mm)	11
D_e (mm)	4.68
β (deg)	30
L_{pp} (mm)	323.6
L_c (mm)	275
W (mm)	94.3

allowing for observation and video acquisition of the flow. The window thickness is 12.7 mm.

The PHE was mounted vertically and the flow directed upwards, as indicated by the red arrows in Fig. 2. Dilute solutions of sodium bicarbonate and acetic acid were fed into the reactor at the inlet port, subsequently mixing and initiating the reaction. Fig. 3 shows the flow loop layout for the reactor, which consists of two circuits for the sodium bicarbonate solutions that can be operated independently to adjust the molar ratios. Each of the two flow loops features a turbine flow meter and a centrifugal feed pump (Tuthill, Alsip, IL) controlled by a 10-turn potentiometer. The window is tapped with 5 instrumentation ports to which diaphragm absolute pressure transducers with a 50-psi ceiling were attached. The uncertainties provided by the manufacturer for the above-stated instruments are tabulated in Table 2.

The pressure transducers and flow meters interface with a digital data acquisition system comprised of National Instruments' SCXI series data acquisition cards (1102 for the pressure transducers and 1126 for the flow meters), which is in turn controlled by a LabVIEW® virtual instrument (VI) (National Instruments, Austin, TX) for data logging and real-time monitoring. High-speed video was acquired with a Phantom V4.2® camera (Vision Research, Wayne, NJ) fitted with a 100 mm Macrovision lens (Carl Zeiss, Germany). The camera was positioned approximately 0.2 m from the front of the acrylic window.

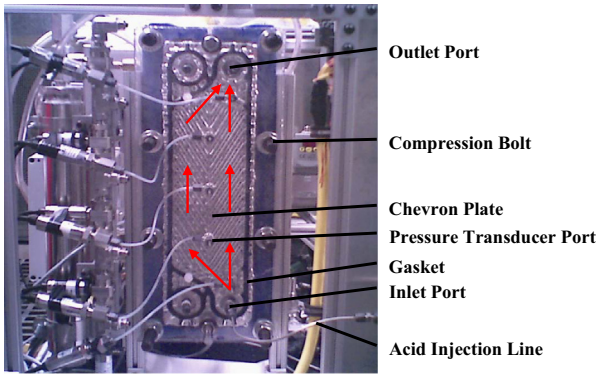

Fig. 2. Front view of HEX reactor.

2.3. Procedure

The effects of flow rate and molar concentrations of reacting species on the flow pattern and pressure profile within the PHE channel were evaluated. The chemical solutions were mixed prior to conducting the experiments: 99% sodium bicarbonate (Sigma Aldrich, St. Louis, MO) was dissolved into a 4 L mixture of distilled water and 99% propylene glycol (Sigma Aldrich, St. Louis, MO) to obtain a mass concentration of 20 g/L. The volume fractions of water and propylene glycol were further adjusted to vary the mixture viscosity and thence the range of Reynolds number attainable by the pumps. Acetic acid solutions were mixed in 1 L batches from glacial acetic acid (Sigma Aldrich, St. Louis, MO) and distilled water at volume ratios (acid:water) between 5% and 10%. The relative uncertainties calculated using the Kline–McClintock method [8] were ± 0.44%, 0.60%, and 0.13% for the propylene glycol volume fraction, acid solution volume fraction, and sodium bicarbonate concentration, respectively.

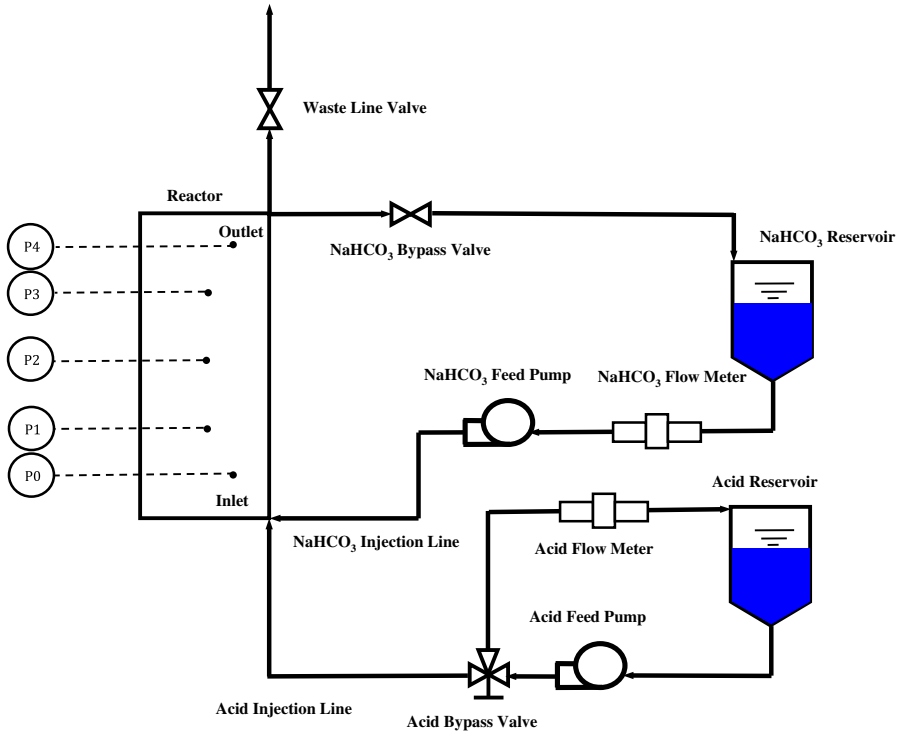

Fig. 3. Flow diagram of HEX reactor; P0-P4 indicate pressure transducer positions.

Table 2
Instrument uncertainty provided by manufacturer.

Instrument name	Manufacturer	Model	Uncertainty (±)
$NaHCO_3$ Flow meter	Omega engineering (Stamford, CT)	FTB2002	3.0% of reading
Acid flow meter	Omega engineering (Stamford, CT)	FTB2002	3.0% of reading
Pressure transducers	Omega engineering (Stamford, CT)	PX409-050A5 V	0.08% of reading

Prior to conducting the experiments, the window surface was polished and coated with a thin layer of carmuaba wax to protect the acrylic resin from the acetic acid. The lines, valves, and flow meters were flushed with distilled water before and after testing to remove contaminants. The following procedure was adopted: the bypass valves on both flow loops were opened, and their respective pumps adjusted until the desired flow rate was obtained for each. During this time, the illumination apparatus and high-speed camera position were adjusted. The pumps were temporarily stopped, the bypass valves closed, and the waste valve opened; the camera and pumps were then triggered simultaneously, during which time the VI recorded pressure and flow rate data while the camera captured images at 1000 frames per second. After 10 s, the acid pump was shut off and the sodium bicarbonate pump was allowed to continue running for an additional 5 s to purge any remaining acid from the chamber. The camera was then adjusted to a new axial position, and the test repeated twice at the same acid and sodium bicarbonate flow rates.

3. Results and discussion

The experiments were conducted by varying the fluid flow rate and the molar ratio between the reacting species. The flow rates ranged from 0.031 to 0.074 L/s; the acid:bicarb molar ratio ranged from 5:2 to 7:10. The conditions for each experiment are tabulated in appendix A.

3.1. Pressure measurements

To establish that the duration of the individual experimental runs were sufficient to permit a statistically steady [9] condition to be reached, the absolute pressure recorded for a representative test set are plotted in Fig. 4 as a function of time elapsed from the test start. The pressure and flow rates undergo a brief startup transient once the acid pump is started, which quickly plateaus after an elapsed time of 5 s, and remains steady until the acid pump is stopped. This behavior was observed for all molar ratios and flow rates considered, so time averaged data obtained from the plateau regions is judged to be representative of the reactor during sustained operation. In the following discussion, all reported values for pressure, flow rate, or molar concentration are with reference to the average value recorded over the steady-state time interval. The molar concentrations of the acetic acid and sodium bicarbonate ($C_{in,\ acid}$ and $C_{in,\ bicarb}$) are derived from the time averaged flow rate of their respective pumps, and a mass balance with the known solution concentrations:

$$C_{in,acid} = S_{acid}\dot{V}_{acid}/\dot{V}_{total} \tag{2}$$

$$C_{in,bicarb} = S_{bicarb}\dot{V}_{bicarb}/M_{bicarb}\dot{V}_{total} \tag{3}$$

where S_{acid} is the acid concentration by volume ("strength"), S_{bicarb} is the mass loading (g/L) of sodium bicarbonate and M_{bicarb} is the molar weight of sodium bicarbonate.

While the low flow rates make it difficult to immediately discern changes in the axial pressure drop due to the reaction, there is a prominent rise in the average absolute pressure in the channel with increasing total flow rate. There are two possible causes for the back pressure rise: increased hydraulic losses in the waste lines and valve, or expansion of gas products within the reactor. Since the hydraulic diameter of the tubing following the reactor outlet is much larger than that of the reactor channels, increased downstream pressure losses appear less likely to be responsible for this phenomenon than the sudden evolution of gas inside the reactor. This is also corroborated by the sudden increase in reactor pressure that occurred immediately after the commencement of the reaction. While the molar ratios are the same for each flow rate, greater amounts of gas are produced by the neutralization reaction as the molar flow rate of both reacting species increases.

This is further confirmed by plotting the outlet pressure (from transducer P4) as a function of the molar flow rate of the limiting reactant (i.e., the reactant with the lower inlet concentration of the two) defined as $\dot{V} \cdot C_{in,\min} = \dot{V} \cdot \min(C_{in,acid}, C_{in,bicarb})$, where $\dot{V}$ is the total flow rate and $C_{in,\min}$ is the inlet concentration of the limiting reactant. The quantity $\dot{V} \cdot C_{in,\min}$ corresponds to the maximum flux of CO_2, in mol/m^2/s, that would be produced assuming that the reaction completed within the channel. Such a plot including all tests is demonstrated in Fig. 5.

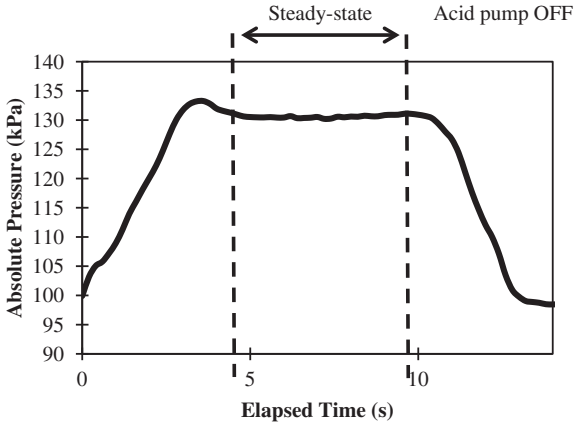

Fig. 4. Transient pressure signal of pressure transducer P0 for test series A1; acid pump is switched on at time = 0 s.

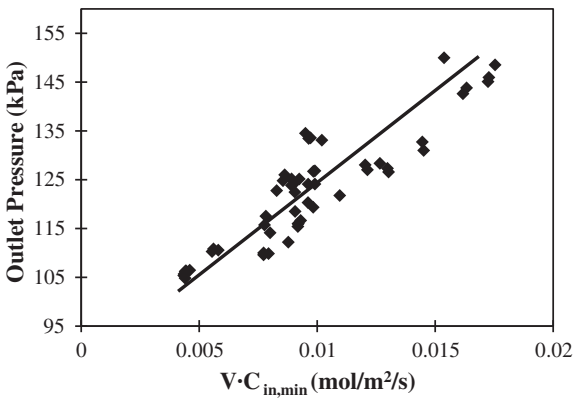

Fig. 5. Time-averaged pressure reading at pressure transducer P4 as a function of maximum molar flux of CO_2.

Although we could not verify the remaining quantity of unreacted species at the reactor outlet, the assumption of (approximately) full conversion within the reactor was checked by measuring the reaction times in a stirred beaker, which were typically 2 or 3 s; the residence times achieved in this study were in the range of 1.5–3 s based on a reactor volume of 101 mL (±1 mL). Additionally, Sahoo and Sata reported reaction half-times that were less than one second [7], and that the kinetics were limited by mixing time. Because of the high degree of agitation occurring in the reactor, and the residence times close to the observed release of gasses in a stirred beaker, it can be concluded that the reaction is most likely very close to completion upon reaching the reactor outlet.

Comparing the change in the values of back pressure rise at different flow rates, it was clear that the frictional and gravitational pressure drop are not significant factors determining the reactor conditions. However, it is well understood that the prediction of thermal performance of heat exchangers is closely tied to the prediction of frictional pressure drop and therefore the utility of the frictional pressure drop measurements in predicting reactor thermal performance will be discussed in Part II of this study.

The absolute pressure data obtained from the outlet was also used to calculate the superficial velocity of the gas phase by using the ideal gas equation of state to obtain the density, and the measured molar flow rate (assuming complete conversion) to obtain the mass flux. Fig. 6 illustrates a plot of superficial gas velocity (U_g, m/s) with respect to gas-phase mass flux (m'', kg/m^3). While U_g increases with greater mass fluxes, dU_g/dm" appears to diminish. The decreasing slope corresponds to an increase in the calculated gas density which arises from the enhancement of the reactor pressure. With increase in mass flux values, the tortuous channel geometry and low hydraulic diameter increasingly impede the escape of the gas (reaction products) from the heat exchanger. This further implies that the gas escape kinetics govern the reactor pressure.

3.2. Flow visualization

The high-speed camera was moved to three fixed axial locations while performing the experiments in a given test series (i.e., fixed molar ratio and flow rate). This enabled the monitoring of the evolution of the two-phase flow in the axial direction with a framing rate of 1000 fps; the field of view was approximately 13 × 26 mm. The camera had 512 × 512 pixel resolution, which was reduced to 256 × 512 to reduce the size of the video files. The similarity between the flow patterns observed in the experiments obviates the need for an exhaustive discussion of each video that was acquired. Instead, a representative video file (obtained from test series B3) was used for the flow pattern analysis.

Over the range of flow rates and molar ratios tested, two distinct flow regimes that were observed: a froth-like flow (Fig. 7a), and a dispersed bubbly flow (Fig. 7b). The froth flow was observed where the reaction was particularly strong, such as near the inlet port after the acetic acid and sodium bicarbonate solutions were mixed. The size of the bubbles decreased as greater reactant concentrations were used, indicating that the bubble size is inversely correlated with the gas evolution rate. Dispersed bubbly flow was typical of lower molar flow rates, or in regions where the reaction had ceased due to complete consumption of one of the reactants. In such cases, there was a wider range of bubble sizes, but all were still much smaller than the furrow width (10 mm) or the maximum channel spacing (4 mm). The difference between these two types of flows shows that the additional agitation produced by the chemical reaction acts to inhibit the formation of larger bubbles. The fine, uniformly distributed bubbles in froth flow also explain the decrease in the gas superficial velocity discussed previously: as the flow becomes more homogenous in nature, the relative velocities between the gas and liquid phase decreases. The violent churning and mixing produced by the reaction 'pulverizes' the flow such that it behaves more as a single fluid. As larger quantities of gas are evolved in the channel, increased collisions between bubbles and the tortuous channel passages also contribute to the homogenizing effect. In no instance were any large gas-continuous flow structures observed, which also supports the aforesaid assertion.

The position of individual bubbles could be tracked on a frame-by-frame basis to reconstruct their flow paths. Due to the similarities between the video footage obtained, the flow paths shown here are representative of the results obtained in this study. Fig. 8 shows the paths of several bubbles tracked over the course of 15–20 frames from various times. Bubbles of different size and shapes can be observed following nearly identical pathways; thus, there is a definite steady flow structure that exists even as the chemical reaction progresses to completion. Fig. 7a and b correspond to the screenshots shown in Fig. 8a and b, respectively.

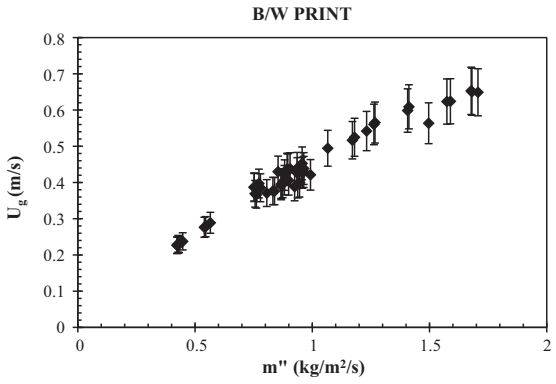

Fig. 6. Superficial velocity of CO_2 at axial position of pressure transducer P4 as a function of maximum gas flux at reactor outlet. The uncertainty for the calculation of U_g obtained with the Kline–McKlintock method [8] was approximately 9%.

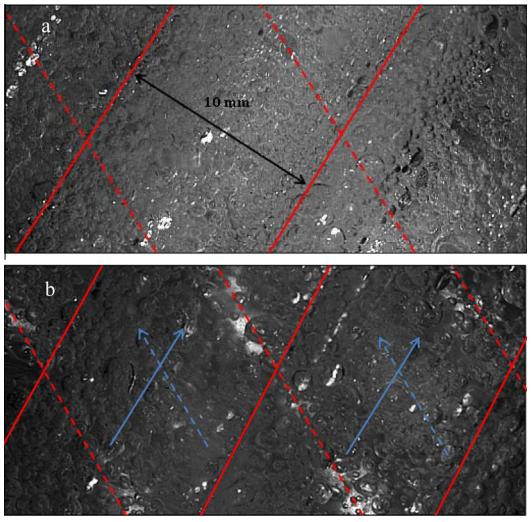

Fig. 7. Screenshots of steady-state operating for test series B3, (b) between P0 and P1; (a) between P2 and P3. Total flow rate: 0.043 L/s; C_{min} = 0.18 [mol/L]. The solid red line represents the crest of a furrow and the dotted red line represents a trough. Blue lines indicate the direction of crossing flow, with the dotted line representing the lower furrow and the solid line the upper furrow. (For interpretation of the references to color in this figure legend, the reader is referred to the web version of this article.)

The pathlines for froth flow compared to those of bubbly flow appear very similar, despite the differences in bubble sizes.

It is also worth noting that the same flow components discussed in the literature [10] for single-phase flow also appear to be present in the two-phase flows studied here. Namely, the 'S'-shaped or abruptly curving pathlines indicate a bubble following a sinusoidal wavy flow pattern (i.e., alternating between upper and lower corrugations in the main flow direction), while others follow the direction of a single corrugation. The fact that the same basic flow components characteristic of single-phase flow in chevron PHEs also exist for two-phase flow is consistent with the observations reported by Tribbe and Müller-Steinhagen [11] for bubbly flow. Because only the bubbles closest to the window could be observed and tracked, the flow fields shown in Fig. 8 do not include bubbles from the entire channel depth. It may be argued, based on symmetry between the upper and lower plates, that the patterns observed in the upper corrugations are similar to those in the lower corrugations.

3.3. Two-Phase Multiplier Assessment

The similarities observed in the flow patterns (bubbles following paths similar to those of single-phase flow) recorded in this study to those reported by Tribbe and Müller-Steinhagen [11] invite a comparison to the two-phase multiplier correlation they proposed from their pressure drop measurements for air–water vertical upward flow in a chevron PHE. In fact, these authors also tested the same model of PHE used in this study (Alpha Laval M3) [11,12]. The two-phase multiplier is defined as:

$$\Phi_{TP}^2 = \left(\frac{dP}{dz^*}\right)_{F,TP} \Big/ \left(\frac{dP}{dz^*}\right)_{F,SP} \tag{4}$$

where the subscript F indicates the frictional pressure drop component, and TP and SP represent two-phase flow and its equivalent (i.e., same mass flux) single-phase flow, respectively. The correlation due to Tribbe and Müller-Steinhagen [12] is as follows:

$$\Phi_{TP} = 1.423 - 0.0724 \ln X + 1.031/X \tag{5}$$

where, X is the Lockhart-Martinelli parameter,

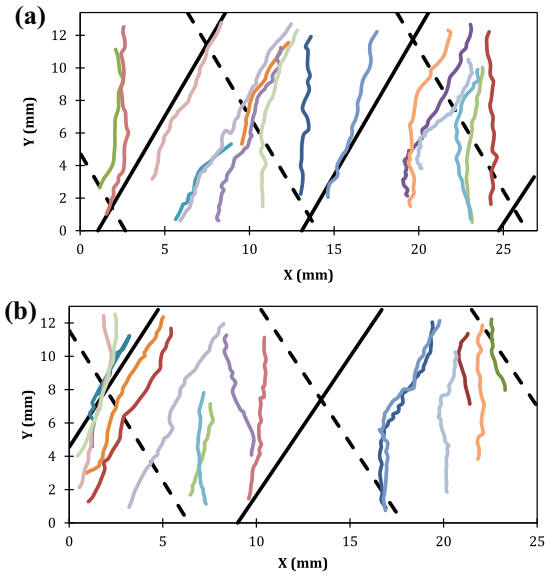

Fig. 8. Pathlines traced from test series B3, (a) between P0 and P1; (b) between P2 and P3. Each colored line corresponds to a particular bubble's path. The solid black lines represent the crest of a furrow and the dotted black lines represent a trough.(For interpretation of the references to color in this figure legend, the reader is referred to the web version of this article.)

$$X = \sqrt{\left(\frac{dP}{dz}\right)_{F,l} \Big/ \left(\frac{dP}{dz}\right)_{F,g}} \tag{6}$$

The authors noted their correlation to be valid over the range $0.06 < X < 10$. When applied locally in a "stepwise manner", Tribbe and Müller-Steinhagen were able to use Eq. (5) to reproduce the total experimental pressure drop within 4% using [12]. We likewise attempted to reproduce the total pressure drop measured during the experiments obtained from the reactor using Eq. (5). In two-phase flow, the total pressure drop is typically expressed in terms of a gravity, acceleration, and friction component [9]:

$$\Delta P = \Delta P_G + \Delta P_A + \Delta P_F \tag{7}$$

where,

$$\Delta P_G = \int_{z_0}^{z_4} g[(1-\alpha)\rho_l + \alpha\rho_g]dz \tag{8}$$

$$\Delta P_A = \int_{z_0}^{z_4} \rho_l U_l^2/(1-\alpha)dz \tag{9}$$

$$\Delta P_F = \int_{z_0}^{z_4} \Phi_{TP}^2\left(\rho_l U_l^2 f/2D_h\right)dz \tag{10}$$

U_l is the equivalent single-phase superficial velocity (m/s) (i.e., as if liquid were flowing alone at the same total mass flux), ρ is the density (kg/m^3), α is the void fraction, f is the single-phase friction factor, and g is the gravitational acceleration (m/s^2). The subscripts l and g signify the liquid phase and the gas phase, respectively. These integrals were evaluated between the position of pressure transducer P0, positioned slightly forward from the inlet port (axial distance z_0), and pressure transducer P4 just before the outlet port (position z_4); a total length of approximately 275 mm as measured parallel to the channel chevron spine. To estimate the void fraction, Kreissig and Müller-Steinhagen [13] recommended a correlation due to Rouhani [14], which was also used here:

$$\alpha = \frac{x}{\rho_g}\left\{[1+0.12(1-x)]\left(x/\rho_g + (1-x)/\rho_l\right) + 1.18/\left(\dot{m}''_{total}\rho_{ls}^{0.5}\right)\left[g\sigma(\rho_l-\rho_g)\right]^{0.25}\right\}^{-1} \tag{11}$$

In this equation, the total mass flux and quality, respectively, are:

$$\dot{m}''_{total} = U_l[\rho_l + M_g C_{in}(1-\eta)] \tag{12}$$

$$x = (1-\eta)(\rho_l/M_g C_{in} + 1 - \eta)^{-1} \tag{13}$$

where, $\eta = C/C_{in}$, C is the mass concentration of the limiting reactant, C_{in} is the value of C at the inlet port, and M_g is the molecular weight of the gas phase (44 kg/kmol for CO_2). In order to simplify the evaluation of the integrals in Eqs. (8)-(10), it was assumed that the gas mass fraction was constant throughout the channel length. This assumption yields the following approximations:

$$\Delta P_G \cong \left[(1-\bar{\alpha})\rho_l + \bar{\alpha}\rho_g\right](z_4 - z_0) \tag{14}$$

$$\Delta P_A \cong \rho_l U_l^2[(1-\bar{\alpha})^{-1} - 1] \tag{15}$$

Since the frictional pressure drop was insignificant compared to the absolute pressure, the density was evaluated at the outlet pressure P4 and room temperature (24 °C) per the ideal gas equation of state.

As an initial assessment of their suitability for gas-evolving reacting flows in chevron plate heat exchangers, Eqs. (5) and (11) are used in a 1-D plug flow reactor model to estimate the pressure drop in the HEX reactor, and compared to the experimental results.

The steady species transport process for a dilute aqueous solution of acetic acid inside the PHE channel may be approximately described by the following relation:

$$\frac{d\eta}{dz} = -(k/U_l)\eta \tag{16}$$

where k is a rate coefficient that will depend on fluid mixing (since the reaction is diffusion limited), and will therefore vary with U_l and turbulence generated by gas bubbles. For the sake of simplifying the calculations, $k/U_l = k^*$ is taken to be a constant (assuming $k \sim U_l$). It is also dependent on temperature, but the experimental conditions are, to a very good approximation, isothermal. As mentioned before, the reaction between aqueous sodium bicarbonate and acetic acid is first order with respect to acetic acid [6] when the release of CO_2 is the rate limiting step [7]. This transport equation may be integrated to obtain:

$$\eta(z) = \exp\{-k^* z\} \tag{17}$$

The assumption in this model is that acetic acid is the rate limiting reactant. Otherwise, to account for the exhaustion of a rate limiting reactant at axial location z^*, a "cut-off" will have to be imposed such that $\eta(z \geqslant z^*) = (C_{in} - C_{\min})/C_{in}$, where C_{min} is the molar concentration of the rate limiting reactant at the inlet. The axial concentration profile is used with the differential forms of Eqs. (7)–(10) to predict the incremental pressure drops over K control volumes of length Δz, which are summed to calculate the total pressure drop. Setting $K = 100$ was sufficient for convergence. It was also determined that setting $k^* = 20$ 1/s gave good agreement with the experimental results – changing k^* to higher values did not improve the agreement, which supports the assumption that the majority of the reaction had completed by the first pressure transducer (P0).

Calculating the appropriate value of the Lockhart–Martinelli parameter (Eq. (6)) required an appropriate single-phase flow correlation. Water/propylene glycol mixtures of 20% and 31.5% propylene glycol by volume were used to obtain a correlation that represents the single-phase behavior of the chevron PHE with the acrylic window installed. For the range $8 \leqslant Re \leqslant 70$, the data could be represented by the relation $f = 24/\mathrm{Re}$ to within an average deviation of ±23% and an expected deviation of ±64% at a 95% confidence level.

It was found that the frictional pressure drops were severely underestimated by Eq. (5). A correction factor of 3.0, which is derived from the average of the ratio between experimental Φ_{TP} values and those predicted by the uncorrected Eq. (5), was introduced to approximately compensate for the simplifying assumptions inherent in Eq. (17). After applying the correction factor to Eq. (5), the total pressure drop was reproduced with errors ranging from 0.7% to 49%, with an average deviation of 26% at 95% confidence. Some of this disagreement may possibly be attributed to the assumption of a constant value of k^* for all of the experiments and the neglect of coupling between mixing, chemical kinetics, and gas–liquid interaction. Representative results comparing the axial pressure distributions measured experimentally and predicted using the method described above (with the correction applied to Eq. (5)) are shown in Fig. 9. The deviations from the expected linear axial pressure profile in Fig. 9 can be attributed to the presence of sudden changes in channel geometry at the distribution zones where pressure transducers P0 and P4 are located. The experimental two-phase multiplier values and the empirically adjusted Eq. (5) are compared in Fig. 10, where the predicted values can be seen to fall within the spread of the experimental values.

Established two-phase flow correlations [11,14], with appropriate empirical adjustment, provided acceptable engineering accuracy for pressure drop calculations. However, the fact that the current two-phase multiplier was significantly higher than that of air–water flow (about 9-fold) points to the need to consider the coupling between chemical kinetics and hydrodynamics if high

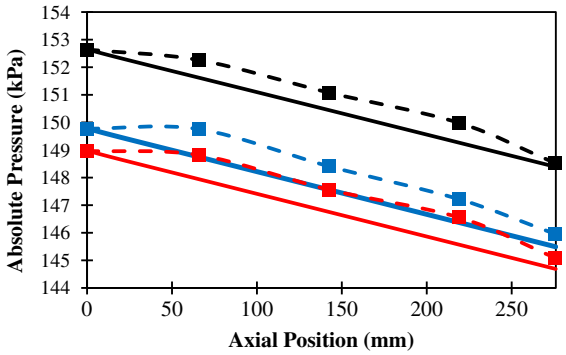

Fig. 9. Axial pressure profiles from test series D1 (dashed line) compared to model predictions (solid lines). Colors differentiate tests with slight differences in flow rate and pressure from the nominal set points to show that the overall pressure drop is repeatable. Markers correspond to axial location of absolute pressure transducers. (For interpretation of the references to color in this figure legend, the reader is referred to the web version of this article.)

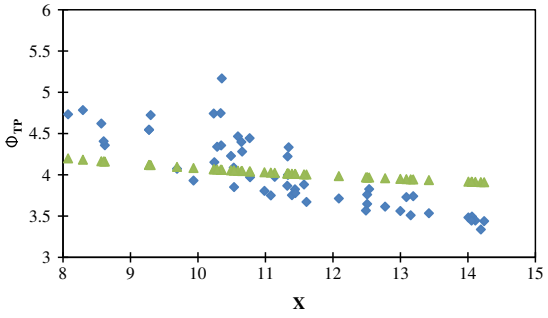

Fig. 10. Comparison of experimentally calculated values (blue diamonds) and predictions Eq. (5) with multiplier adjustment of 3.0 applied, (green triangles) of ΦTP. (For interpretation of the references to color in this figure legend, the reader is referred to the web version of this article.)

fidelity calculations are required. The additional fluid agitation produced by the sudden evolution and expansion of gas within the flow is likely to contribute to considerably higher frictional losses than if the liquid and gas phases were simply injected at the inlet as in references [11,12]. Although the multiplier correction to the two-phase multiplier correlation is unable to fully account for this effect, it is able to provide accuracy sufficient for estimating pressure drop values over the range of Lockhart–Martinelli parameter values (X) considered (between 8 and 14) for the reactor (and reactants) used in this study.

4. Conclusion

In this study, hydrodynamic behavior in a chevron plate heat exchanger with multi-phase flow with chemical reaction (involving gas bubble evolution) is investigated experimentally. The chemical reaction between acetic acid and sodium bicarbonate provided fundamental insights into the reactor hydrodynamics, and guided the selection of hydrodynamic correlations for gas-generating reacting flows. High-speed flow visualization showed that the vigorous reaction has a homogenizing effect on vertical upward gas–liquid flow, preventing the formation of any large heterogeneous flow structures, which supports the use of correlations based on the assumption of homogenous flow. Using the correlation proposed by Tribbe and Müller-Steinhagen [11,12] for the two-phase multiplier, with an empirical correction factor of 3.0, along with the void fraction correlation developed by Rouhani [14], the total pressure drop could be reproduced with a maximum error of 49%. The level of accuracy obtained using these two correlations

was typical for general two-phase flow correlations, suggesting they are appropriate bases for developing empirically adjusted relations for estimating pressure drop and void fraction in PHEs with gas-generating reacting flows.

Disclosure Statement

To our knowledge, there are no conflicts of interest between the authors or their respective institutions with the International Journal of Heat and Mass Transfer

Appendix A. Test matrix

The following table lists the experimental parameters for each test set and constituent series. The flow rates are average readings during the steady-state 'plateau' time interval.

List of experimental parameters for each test set and constituent series. The flow rates are average readings during the steady-state 'plateau' time interval.

Test series	A1	A3	A4	A5	A6	A7
Test set A						
Acid strength	5%	5%	5%	5%	2.35%	2.35%
Bicarb loading (g/L)	20	20	20	20	25	25
Total flow rate (L/s)	0.064	0.072	0.074	0.065	0.041	0.032
Cin, acid (mol/L)	0.14	0.13	0.13	0.14	0.14	0.14
Cin, bicarb (mol/L)	0.2	0.2	0.2	0.2	0.2	0.2
Test set B						
	B1	B2	B3	B4		
Acid strength	5%	5%	5%	5%		
Bicarb loading (g/L)	20	20	20	20		
Total flow rate (L/s)	0.058	0.049	0.042	0.07		
Cin, acid (mol/L)	0.18	0.19	0.2	0.18		
Cin, bicarb (mol/L)	0.19	0.19	0.18	0.19		
Test set C						
	C1	C2	C3			
Acid strength	5%	5%	5%			
Bicarb loading (g/L)	20	20	20			
Total flow rate (L/s)	0.068	0.055	0.031			
Cin, acid (mol/L)	0.35	0.34	0.35			
Cin, bicarb (mol/L)	0.14	0.14	0.14			
Test set D						
	D1	D2	D3	D4		
Acid strength	8%	8%	7%	7%		
Bicarb loading (g/L)	30	30	31.4	31.4		
Total flow rate (L/s)	0.063	0.053	0.061	0.037		
Cin, acid (mol/L)	0.32	0.33	0.37	0.4		
Cin, bicarb (mol/L)	0.28	0.27	0.26	0.25		

References

[1] Z. Anxionnaz, M. Cabassud, C. Gourdon, P. Tochon, Heat exchanger/reactors (HEX reactors): concepts, technologies: state-of-the-art, Chem. Eng. Process.: Process Intensificat. 47 (2008) 2029–2050.

[2] D. Johnson, S. Patnaik, J. Ervin, An integrated chemical reactor-heat exchanger based on ammonium carbamate, in: Proceedings of the SAE 2012 Power Systems Conference, SAE International, Phoenix, 2012.

[3] W.W. Focke, J. Zachariades, The effect of the corrugation inclination angle on the thermohydraulic performance of plate heat exchangers, Int. J. Heat Mass Transfer 28 (1985) 1469–1479.

[4] W.W. Focke, Turbulent convective transfer in plate heat exchangers, Int. Commun. Heat Mass Transfer 10 (1983) 201–210.

[5] W.W. Focke, Asymmetrically corrugated plate heat exchanger plates, Int. Commun. Heat Mass Transfer 12 (1985) 67–77.

[6] B. Parkash, Reaction of RCOOH–$NAHCO_3$, a convenient illustration, Resonance (1998) 89–95.

[7] P. Sahoo, B. Saha, Inadequacy of water band movement technique for kinetic interpretation of RCOOH–$NAHCO_3$ reaction, Resonance (1999) 65–71.

[8] S.J. Kline, F.A. McClintock, Describing uncertainties in single-sample experiments, Mech. Eng. 1 (1953) 3–8.

[9] J.G. Collier, J.R. Thome, Convective Boiling and Condensation, third ed., Oxford University Press, New York, 1996.

[10] H. Martin, A theoretical approach to predict the performance of chevron-type plate heat exchangers, Chem. Process.: Process Intensificat. 35 (1996) 301–310.

[11] C. Tribbe, H.M. Müller-Steinhagen, Gas/Liquid flow in plate-and-frame heat exchangers – Part II: two-phase multiplier and flow pattern analysis, Heat Transfer Eng. 22 (2001) 12–21.

[12] C. Tribbe, H.M. Müller-Steinhagen, Gas/Liquid flow in plate-and-frame heat exchangers - part I: pressure drop measurements, Heat Transfer Eng. 22 (2001) 5–11.

[13] G. Kreissig, H.M. Müller-Steinhagen, Frictional pressure drop for gas/liquid two-phase flow in plate heat exchangers, Heat Transfer Eng. 13 (1992) 42–52.

[14] S.Z. Rouhani, E. Axelsson, Calculation of void volume fraction in the subcooled and quality boiling regions, Int. J. Heat Mass Transfer 13 (1970) 383–393.